Mon. Not. R. Astron. Soc. **000**, 000–000 (2001)

A small area faint KX redshift survey for QSOs in the ESO Imaging Survey *Chandra* Deep Field South.

Scott M. Croom[1,2⋆], S. J. Warren[1], K. Glazebrook[2,3]
[1] *Astrophysics Group, Imperial College of Science, Technology and Medicine, Blackett Laboratory, Prince Consort Road, London, SW7 2BW*
[2] *The Anglo-Australian Observatory, PO Box 296, Epping, NSW 2121, Australia.*
[3] *Department of Physics & Astronomy, Johns Hopkins University, 3400 North Charles Street, Baltimore, MD 21218-2686, USA.*

25 July 2001

ABSTRACT

In this paper we present preliminary spectroscopic results from a small area faint K-excess (KX) survey, and compare KX selection against UVX selection. The aim of the KX method is to produce complete samples of QSOs flux-limited in the K band, in order to minimize any selection bias in samples of QSOs from the effects of reddening and extinction. Using the photometric catalogue of the ESO Imaging Survey *Chandra* Deep Field South (48 arcmin^2) we have identified compact objects with $J-K$ colours redder than the stellar sequence, that are brighter than $K=19.5$. We have obtained spectra of 33 candidates, using the LDSS++ spectrograph on the AAT. Amongst the 11 bluer candidates, with $V-J<3$, three are confirmed as QSOs. Identification of the 22 redder candidates with $V-J\geq 3$ is substantially incomplete, but so far no reddened QSOs have been found. Near-infrared spectroscopy will be more effective in identifying some of these targets. Only two UVX ($U-B<-0.2$) sources brighter than $K=19.5$ are found which are not also KX selected. These are both identified as galactic stars. Thus KX selection appears to select all UVX QSOs. The surface density of QSOs in the blue subsample ($V-J<3$) at $K\leq 19.5$ is 325^{+316}_{-177} deg^{-2}. Because identification of the red subsample ($V-J\geq 3$) is substantially incomplete, the 2σ upper limit on the density of reddened QSO is large, <1150 deg^{-2}. As anticipated, at these faint magnitudes the KX sample includes several compact galaxies. Of the 14 with measured redshifts, there are roughly equal numbers of early and late type objects. Nearly all the early type galaxies are found in a single structure at $z=0.66$.

Key words: surveys – infrared: galaxies – galaxies: active – quasars: general

1 INTRODUCTION

The most commonly used method for finding QSOs utilizes the fact the QSOs are bluer than most stars at ultra-violet wavelengths. This ultra-violet excess led to the UVX technique (e.g. Schmidt & Green 1983), which in its simplest form uses the blue $U-B$ colours of QSOs to differentiate them from stars. This and related methods have been utilized in most of the largest QSO surveys to date (e.g. Durham/AAT, Boyle et al. 1990; 2dF, Croom et al. 2001). Warren, Hewett & Foltz (2000) have recently proposed the KX technique for producing K-band flux limited samples of QSOs: because of the power-law nature of their spectra, not only are QSOs bluer than stars at UV wavelengths, but also redder than stars at near-infrared wavelengths. In considering the KX technique it is important to distinguish between the two effects of reddening and extinction (e.g. Binney & Merrifield 1998). KX QSO samples could be useful in overcoming selection biases from both effects. First, the KX method is insensitive to reddening. That is, the reddening vector in the $V-J$ vs. $J-K$ plane does not drive QSOs towards the stellar locus. So the KX method could detect QSOs that have been missed in a survey based on UV-optical colours because they are unusually red, even though they are brighter than the flux limit. Second, reddened QSOs suffer greater extinction at short wavelengths and so can fall below the optical flux limit, but could be detected in the K band. More generally, since red QSOs are under-represented in surveys at short wavelengths, and similarly blue QSOs are under-represented in surveys at long wavelengths, it is clear that surveys at two widely separated wavelengths are

⋆ scroom@aaoepp.aao.gov.au

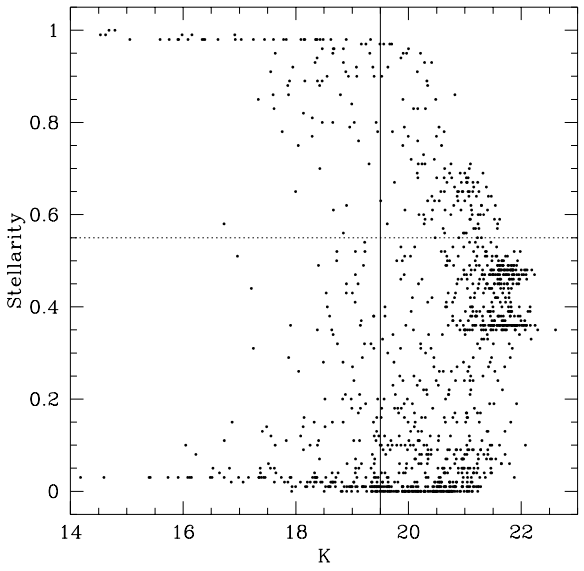

Figure 1. The stellarity index for all K-band sources from the SExtractor catalogue of Rengelink et al. (1998). The flux limit of the sample, $K = 19.5$ mag is marked with the solid vertical line. The stellarity limit of 0.55 is shown by the dotted line.

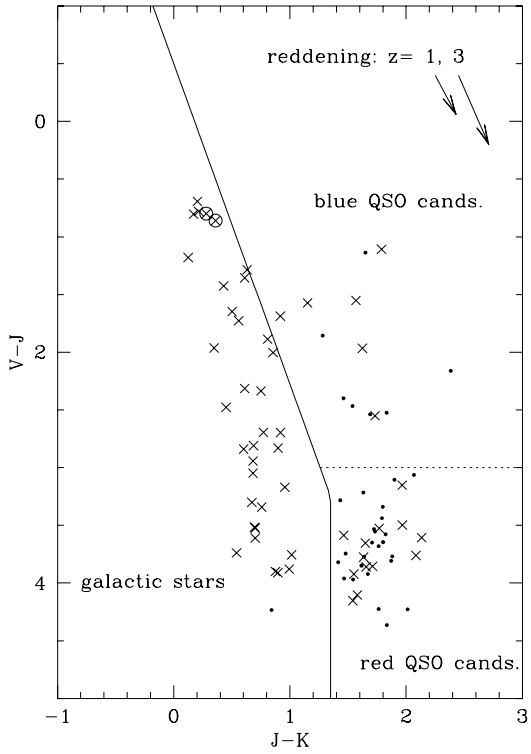

Figure 2. Colour-colour plot in $(V-J)$ vs. $(J-K)$ for $K \leq 19.5$ objects with stellarity ≥ 0.55 (points). The crosses denote objects with stellarity ≥ 0.90. The selection limits for our KX sample are shown by the solid line, while the blue and red candidate subsamples are separated by the dotted line. The two UVX candidates which are not KX selected are circled. In the top right-hand corner we plot the reddening vectors for absorbers at $z = 1$ and 3 for $E(B-V) = 0.1$ using the LMC extinction curve.

necessary to characterize fully the optical-infrared emission from QSOs.

There is currently considerable interest in quantifying the numbers of red QSOs. Red QSOs have been discovered in radio selected samples (Webster et al. 1995), and highly absorbed QSOs have been invoked to explain the spectrum of the X-ray background radiation (e.g. Madau et al. 1994). The unified model of AGN (e.g. Antonucci 1993) postulates a dusty torus surrounding the central black hole engine. At high inclination angles, when observing through the torus, the gas associated with the torus will absorb soft X-rays, hardening the intrinsic QSO spectrum such that it can be reconciled with the harder X-ray background. The dust also preferentially extinguishes blue optical/UV flux, reddening the object at optical wavelengths. A small number of these "type 2 QSOs" have been discovered (e.g. Almaini et al., 1995; Boyle et al., 1998) in deep X-ray samples, showing narrow emission lines in the optical, but broad lines in the near-infrared (IR). One way to reduce the bias against selecting such objects is to construct an IR selected sample (alternatives would be to use hard X-ray or deep radio surveys).

As well as intrinsic absorption, QSOs may also suffer extinction and reddening by dusty objects which lie along their line of site. For example, a dusty damped Lyman α absorber (DLA) will have the effect of making the background QSO both fainter and redder (Fall & Pei 1993). A bias will then be introduced in the distribution of DLAs detected from optically selected QSO samples. This bias is apparent as a lack of high H I column ($\log N$[H I]> 21), high metallicity DLAs (Boissé et al. 1998). A second example is that of gravitational lenses. QSOs behind a dusty lens are less likely to be detected, potentially biasing low the number of gravitational lenses found. This will have a significant impact on the cosmological interpretation of the number of gravitationally lensed QSOs.

This paper reports on a test of the KX method. Candidate QSOs are stellar sources with $J-K$ colours redder than the stellar sequence in a $V-J$ vs. $J-K$ two-colour diagram. Because of the small areas so far covered by surveys in the near-infrared, to produce a QSO sample of significant size we decided to go deep, rather than wide. The advantage of this strategy is that we can use multi-object spectroscopy for candidate confirmation. The main disadvantage is that the list of candidates will be contaminated by compact galaxies, which is not a significant problem at bright magnitudes. This is made worse by the fact that faint QSOs may also be resolved, so that the position of the star/galaxy discrimination boundary must be relaxed, in order for the sample to be complete. Section 2 describes the photometric data, and the candidate selection procedure employed. Section 3 presents the spectroscopic observations which were carried out with LDSS++ at the Anglo-Australian Telescope. We discuss our results in Section 4.

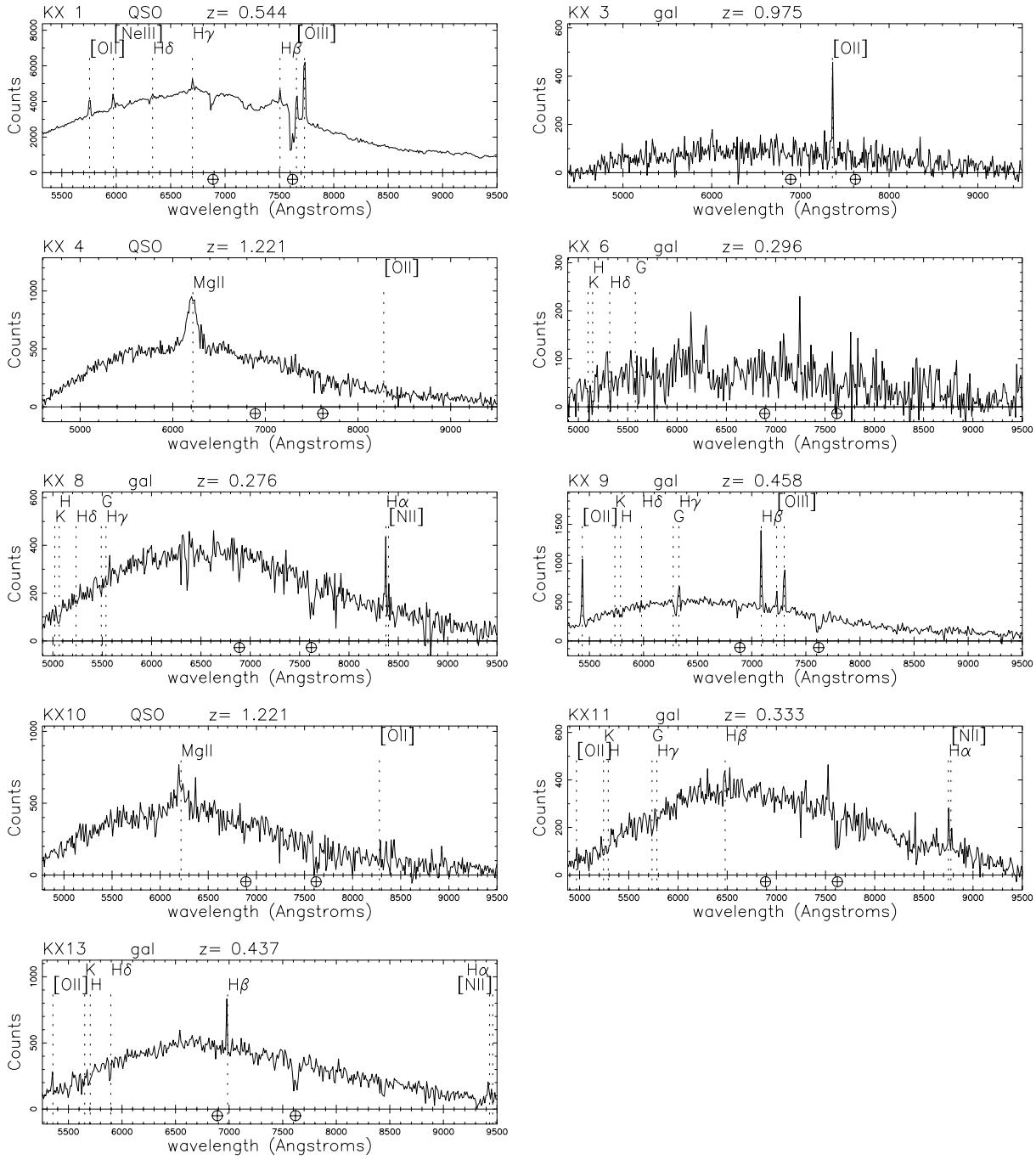

Figure 3. Spectra of the identified objects in the blue subsample. The wavelengths of spectral features are labelled on each spectrum. We have not corrected for telluric absorption bands, and indicate these by a circled cross.

Table 1. KX selected objects and spectroscopic identifications for the blue sub-sample, ($V - J \leq 3.0$). The magnitudes are listed in the $UBVRJK$ bands and S/G_K denotes the SExtractor stellarity parameter in the K band. Objects with an ID of "-" have not been observed. Those with a "?" ID could not be identified from their spectra. An (e) or (a) after a "gal" ID denotes emission or absorption dominated spectra respectively. The observed spectral features, in both absorption and emission are also listed.

name	RA(J2000)	Dec.(J2000)	U	B	V	R	J	K	S/G_K	z	ID	spectral features
KX1	3 32 08.70	–27 47 34.5	18.90	19.23	18.64	18.44	17.07	15.92	0.98	0.544	QSO	[O II],[Ne III],Hδ,Hγ,Hβ,[O III]
KX2	3 32 09.48	–27 48 06.9	22.58	21.67	20.69	20.37	19.01	18.09	0.98	0.000	-	
KX3	3 32 16.53	–27 44 49.2	23.13	23.84	23.16	22.73	20.76	19.30	0.71	0.975	gal(e)	[O II]
KX4	3 32 30.02	–27 45 30.2	20.54	21.53	21.33	21.03	20.22	18.43	0.98	1.221	QSO	Mg II,[O II]
KX5	3 32 30.11	–27 45 24.0	22.78	23.52	23.02	22.50	20.50	18.67	0.61	0.000	?	
KX6	3 32 31.51	–27 46 23.4	-	24.17	23.58	22.80	21.42	19.04	0.80	0.296	gal(a)	H,K,Hδ,G
KX7	3 32 33.06	–27 46 09.1	23.92	24.10	22.80	21.85	20.33	18.79	0.86	0.000	?	
KX8	3 32 33.58	–27 46 23.8	22.61	23.05	21.98	21.38	20.12	18.84	0.56	0.276	gal(e)	H,K,Hδ,G,Hγ,Hα,[N II]
KX9	3 32 38.83	–27 47 32.5	21.19	22.11	21.50	20.80	19.95	18.38	0.94	0.458	gal(e)	[O II],H,K,Hδ,G,Hγ,Hβ,[O III]
KX10	3 32 39.13	–27 46 02.1	20.58	21.55	21.21	20.77	20.07	18.42	0.88	1.221	QSO	Mg II,[O II]
KX11	3 32 41.80	–27 46 19.7	24.01	23.98	22.36	21.40	19.82	18.13	0.82	0.333	gal(e)	[O II],H,K,G,Hγ,Hβ,Hα,[N II]
KX12	3 32 44.24	–27 47 33.8	22.46	23.28	22.66	21.80	20.70	19.07	0.92	0.000	-	
KX13	3 32 45.15	–27 47 24.2	22.58	22.99	21.92	20.90	19.37	17.64	0.95	0.437	gal(e)	[O II],H,K,Hδ,Hβ,Hα,[N II]

2 PHOTOMETRIC DATA AND CANDIDATE SELECTION

The photometric data used was that of the ESO Imaging Survey *Chandra* Deep Field South (EIS-CDFS; formally the EIS-AXAF deep field) (Rengelink et al. 1998). The EIS-CDFS deep field covers an area of 48arcmin^2, and was observed in 7 bands $UBVRIJK$ at the New Technology Telescope (NTT) using the SUSI2 and SOFI instruments. The I band coverage of the field is incomplete. Rengelink et al. produced catalogues of detections in each band using SExtractor (Bertin & Arnouts 1996), which generates positions, fluxes, magnitudes and a number of other image parameters including a star-galaxy discrimination parameter. The 2σ magnitude limits are $U \simeq 25.2$, $B \simeq 27.0$, $V \simeq 26.5$, $R \simeq 26.3$, $I \simeq 25.6$, $J \simeq 23.6$ and $K \simeq 21.6$. The data are publicly available from `http://www.eso.org/eis`.

Beginning with the K catalogue we selected all objects brighter than $K = 19.5$, and then picked out the relevant photometry from the V and J catalogues. Unfortunately at these faint magnitudes QSOs may appear non-stellar. Therefore the selection of the star-galaxy discrimination boundary involves balancing the competing requirements of completeness of the QSO sample, and contamination by galaxies. We have included candidates that are marginally non-stellar, applying a cut on the K-band SExtractor stellarity parameter ≥ 0.55, where stellarity = 1 denotes a star and stellarity = 0 denotes a galaxy. Fig. 1 shows the stellarity index plotted as a function of K magnitude together with our selection limits. As illustrated in Fig. 2, all but one of the objects lying in the stellar locus of the two-colour diagram have stellarity ≥ 0.9, so our applied cut is quite conservative. We can anticipate, therefore, that our candidate list will include several galaxies. The KX and UVX methods have this problem in common at faint magnitudes. The KX colour selection was carried out in the $(V - J)$ vs. $(J - K)$ plane, as shown in Fig. 2. Compact objects which have $(J - K) > 1.35$ or $(J - K) > 0.36(V - J) + 0.18$ were selected for follow up spectroscopy. This selection is almost identical to that used by Warren et al. (2000). We make a comparison to UVX selection by finding the $U - B$ colours for all our compact $K < 19.5$ sources. Of those sources with positive detections in the U and B bands only two are found to be selected as UVX ($U - B < -0.2$) and not KX. A further 18 sources are selected as both UVX and KX. The non-KX UVX sources have similar colours in both the optical and IR, these are typical of blue (e.g. A/B) stars. They lie at the blue end of the stellar locus in the $(V - J)$ vs. $(J - K)$ plane (the circled points in Fig. 2).

We divided our KX candidate list into two sub-samples, either side of $(V - J) = 3$. Table 1 lists the 13 objects in the bluer of the two sub-samples, which lie in the same region of the colour-colour plane as typical blue optically selected QSOs. These candidates have average $R = 21.3$. Table 2 lists the 41 objects in the red sub-sample, containing candidate highly reddened QSOs. These candidates have average $R = 22.7$. This sub-sample is expected to be contaminated by compact distant early-type galaxies.

3 SPECTROSCOPIC OBSERVATIONS

Spectroscopic observations were carried out with the Low Dispersion Survey Spectrograph (LDSS++) on the nights of the 11th and 12th of December 1999. LDSS++ uses the MITLL3 CCD, along with a volume phase holographic grism to give very high efficiency ($\sim 25\%$ at 7000Å). Two masks were observed, each containing ~ 45 slits of length $6''$ and width $1.5''$. Faint objects, where possible, were included in both masks. Priority was given to the blue sub-sample, resulting in 11 of the 13 objects being allocated slits, while a smaller fraction (22 out of 41) of the red sub-sample was allocated slits. We were also able to allocate a slit to one of the two non-KX UVX candidates. To fill in the remain-

Table 2. KX selected objects and spectroscopic identifications for the red sub-sample, ($V - J > 3.0$). The format is the same as that in Table 1.

name	RA(J2000)	Dec.(J2000)	U	B	V	R	J	K	S/G_K	z	ID	spectral features
KX14	3 32 06.48	−27 47 28.8	23.53	23.95	22.89	22.32	19.67	18.04	0.75	0.000	-	
KX15	3 32 06.61	−27 46 23.1	-	26.02	25.35	23.90	21.13	19.11	0.76	0.000	-	
KX16	3 32 08.70	−27 45 02.0	25.45	25.64	23.63	22.38	19.71	18.16	0.98	0.000	-	
KX17	3 32 10.57	−27 46 29.1	-	-	-	-	21.49	19.45	0.78	0.000	?	
KX18	3 32 11.26	−27 45 33.7	-	26.66	24.54	23.74	20.39	18.84	0.96	0.333	gal(e)	Hβ,[O III],Hα
KX19	3 32 11.65	−27 45 54.4	-	25.94	25.02	23.34	19.97	18.47	0.80	0.000	-	
KX20	3 32 12.24	−27 45 30.3	24.77	24.92	22.60	21.54	19.32	17.89	0.89	0.000	?	
KX21	3 32 12.50	−27 47 29.3	-	25.61	24.53	23.31	20.42	18.84	0.93	0.000	?	
KX22	3 32 13.05	−27 46 38.2	-	-	-	24.64	20.85	19.31	0.95	0.212	gal(a)	H,K,Hδ,G,Hβ,[O III]
KX23	3 32 14.48	−27 46 24.8	-	25.26	23.94	22.66	20.36	18.89	0.98	0.000	?	
KX24	3 32 14.82	−27 44 33.4	25.73	-	25.38	23.84	21.15	19.39	0.90	0.000	-	
KX25	3 32 15.56	−27 45 36.5	-	26.25	24.85	23.47	20.49	18.66	0.80	0.000	?	
KX26	3 32 16.57	−27 47 27.4	-	25.50	23.51	22.33	19.77	18.29	0.77	0.000	-	
KX27	3 32 17.23	−27 46 49.4	-	26.89	24.50	23.13	20.53	18.99	0.84	0.000	?	
KX28	3 32 17.80	−27 47 15.1	-	25.57	23.23	22.06	19.41	18.00	0.65	0.000	-	
KX29	3 32 18.49	−27 45 56.2	-	25.35	23.35	22.05	19.43	17.76	0.78	0.000	-	
KX30	3 32 18.90	−27 47 34.6	-	27.11	24.33	23.13	20.75	18.93	0.90	0.000	?	
KX31	3 32 19.27	−27 46 32.4	-	25.67	23.32	22.11	19.47	17.86	0.88	0.000	?	
KX32	3 32 19.90	−27 47 21.4	-	26.47	23.98	22.73	20.12	18.47	0.96	0.000	-	
KX33	3 32 19.96	−27 48 31.2	-	25.53	24.07	22.82	20.30	18.66	0.96	0.000	-	
KX34	3 32 20.51	−27 47 32.5	25.10	25.24	23.30	22.37	20.19	18.29	0.81	0.000	-	
KX35	3 32 24.42	−27 46 24.6	-	26.08	24.33	23.28	20.37	18.90	0.62	0.000	?	
KX36	3 32 26.71	−27 46 59.3	-	26.33	24.49	23.14	20.72	19.08	0.90	0.000	?	
KX37	3 32 28.49	−27 47 04.0	24.06	24.85	23.23	21.84	19.58	17.87	0.86	0.668	gal(a)	[O II],H,K,G,Mgb
KX38	3 32 28.79	−27 46 20.7	-	24.32	23.24	22.08	19.71	17.95	0.92	0.000	?	
KX39	3 32 29.27	−27 47 07.8	25.17	25.11	23.12	21.63	19.26	17.55	0.91	0.668	gal(a)	H,K,Hδ,G,Hγ,Hβ,Mgb
KX40	3 32 29.99	−27 47 57.4	-	25.63	24.09	22.96	21.02	18.96	0.79	0.000	-	
KX41	3 32 30.07	−27 47 27.1	24.50	24.65	24.90	24.61	21.29	19.16	0.97	0.000	-	
KX42	3 32 30.89	−27 46 22.1	24.02	24.74	23.96	23.10	20.30	18.66	0.95	0.000	?	
KX43	3 32 31.26	−27 45 33.1	-	-	-	24.33	21.39	19.42	0.80	0.000	-	
KX44	3 32 32.09	−27 44 52.1	24.98	25.48	24.15	22.85	20.34	18.47	0.89	0.000	-	
KX45	3 32 33.89	−27 46 00.6	24.78	-	25.21	24.71	21.45	19.37	0.92	0.000	?	
KX46	3 32 35.80	−27 47 59.1	-	25.09	22.78	21.37	19.10	17.33	0.85	0.665	gal(a)	H,K,Hδ,G,Hγ
KX47	3 32 37.35	−27 47 29.6	-	24.81	22.37	20.99	18.61	16.73	0.58	0.669	gal(a)	[O II],H,K,G,Hγ
KX48	3 32 38.30	−27 44 55.4	-	26.08	23.68	22.28	20.15	18.43	0.70	0.666	gal(a)	H,K,G,Hγ
KX49	3 32 38.83	−27 46 49.2	-	25.70	23.67	22.12	20.12	18.38	0.89	0.000	-	
KX50	3 32 38.83	−27 44 49.3	-	25.65	23.81	22.40	20.31	18.34	0.93	0.000	-	
KX51	3 32 39.27	−27 47 58.6	25.39	25.54	23.04	21.68	19.40	17.60	0.86	0.000	-	
KX52	3 32 40.71	−27 47 31.2	23.98	24.76	23.30	22.05	19.96	18.16	0.89	0.667	gal(e)	[O II],H,K,G,Hβ,[O III]
KX53	3 32 41.45	−27 47 17.4	-	24.93	22.84	21.53	19.40	17.61	0.83	0.000	?	
KX54	3 32 47.38	−27 46 27.3	-	26.21	24.61	23.45	21.46	19.49	0.97	0.000	-	

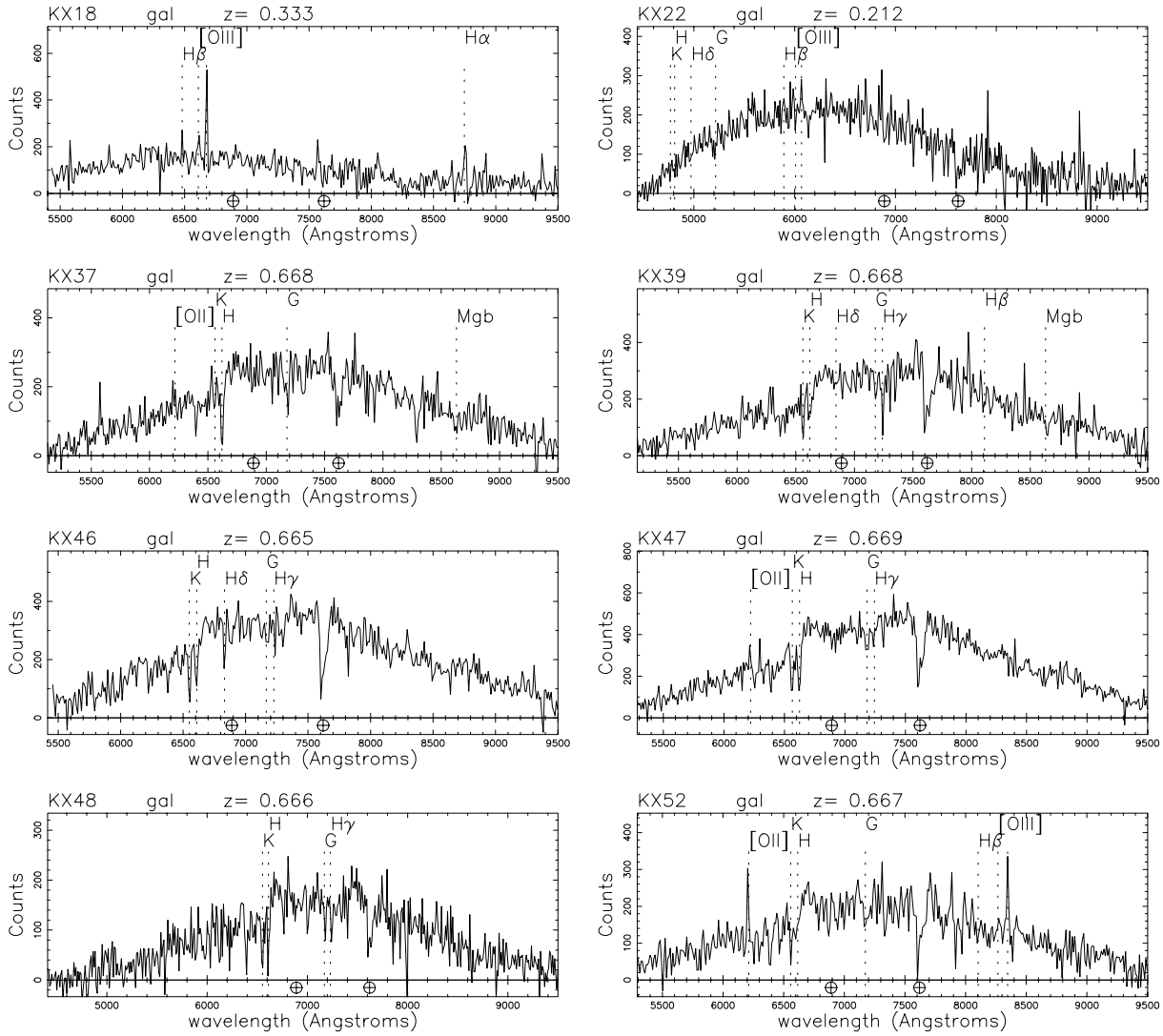

Figure 4. Spectra of the identified objects in the red subsample.

ing space, in positions where there were no KX objects, we randomly selected $K \leq 19$ galaxies (stellarity ≤ 0.1).

The nod-and-shuffle technique was used to optimize sky subtraction (Glazebrook & Bland-Hawthorn 2001). The principle of the method is to quasi-simultaneously record the sky local to the object through exactly the same light path as the object flux, so that the sky can be subtracted. This is in contrast to the usual method which is to subtract a smooth function fit to the sky counts at each wavelength. The telescope was nodded back and forth every 30 seconds by $3''$, keeping the object in the slit. At the same time, the charge was shuffled up and down the CCD, such that a single read out contained two sets of spectra, one for each position of the object in the slit. By simply subtracting one set of spectra from the other, near perfect (i.e. Poisson limited) sky removal is obtained, as the sky flux passes through the same part of the slit, and is incident on the same pixel in the CCD as the object flux. Although the subtraction process increases the sky noise by $\sqrt{2}$, compared to the usual method, the greatly reduced systematic errors allow reliable spectroscopy of much fainter objects.

During the first night of observations we obtained 5×2000s exposures on mask 1, in seeing of $\sim 2''$. On the second night, 7×2000s exposures were obtained on mask 1 in $1 - 1.5''$ seeing and 3×2000s exposures were obtained on mask 2. Copper-Helium-Neon arcs were taken at intervals throughout the night to wavelength calibrate the spectra.

The CCD reduction, spectral extraction and calibration was carried out within the IRAF package, using the tasks within IMRED.CCDRED and IMRED.SPECRED. After bias subtracting the images and interpolating over bad pixels and columns, the images were combined in groups of 2 or 3, averaging and using clipping algorithms to remove cosmic ray events. Combining in small groups, rather than over a whole night, ensured no smearing out of the spectra due to small shifts (typically a fraction of a pixel) caused by flexure in the spectrograph. Each combined frame was split in half, separating the spectra taken at the two nod-and-shuffle positions. One of these two halves was then subtracted from the other to produce the sky subtracted image containing both positive and negative spectra for each object. The routine APEXTRACT was then used to trace and extract the

positive and negative spectra. A number of the spectra have extremely low S/N and were therefore impossible to trace. In these cases the trace used was one interpolated from surrounding well traced spectra. Wavelength calibration was done using the IDENTIFY and DISPCOR routines. Finally, multiple spectra of the same object were combined together.

Classification and redshift determination were undertaken by eye using a modified version of the REDSHIFT program by Karl Glazebrook. A high fraction of the blue sub-sample could be identified (9 of 11 observed), while the redder sub-sample had a much lower identification rate (only 8 of 22), as expected given their much fainter R-band fluxes. The positions, magnitudes, identifications, and redshifts are given in Tables 1 and 2 for the blue and red sub-samples respectively, and the spectra are shown in Figs. 3 and 4. The two UVX selected objects are listed in Table 3. We obtained a spectrum of UVX1 and it was found to be an A star, with clear Balmer absorption lines. The $K \leq 19$ galaxy sample is listed in Table 4 and the galaxy spectra are shown in Fig. 5.

The KX objects are plotted in the $(V-J)$ vs. $(J-K)$ plane in Fig. 6. We identify 3 QSOs; one at $z = 0.544$ and a pair of QSOs at $z = 1.221$. All 3 objects would also be selected in a UVX sample, having colours $(U-B) = -0.33$, –0.99 and –0.97 for KX1, KX4 and KX10 respectively. KX1 also shows narrow Hβ superimposed on a much broader underlying component. The spectra of the $z = 1.221$ QSO pair and their flux ratio are shown in Fig. 7. This pair has an angular separation of $125''$. The ratio of the two spectra is flat over the entire spectroscopic range (Fig. 7c). They also have similar fluxes in all the optical and IR bands. However, the large angular separation makes this pair an unlikely candidate for a gravitational lens.

The remaining identifications are all galaxies, with roughly equal numbers of early and late type spectra (by early and late we mean spectra that are dominated by absorption and emission lines respectively). The early type objects are on average redder. The redshift distribution of the identified galaxies and QSOs is shown in Fig. 8. While the narrow emission line galaxies are distributed from $z \simeq 0.15$ to 1.0, 5 out of 7 of the early type galaxies lie at $z \simeq 0.66$, suggesting the presence of a galaxy cluster at that redshift.

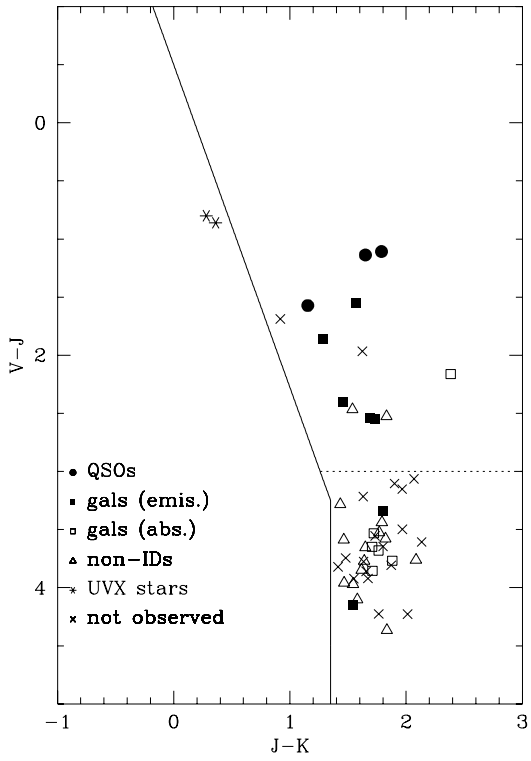

Figure 6. Colour-colour plot in $(V-J)$ vs. $(J-K)$ for our KX selected sample. Different symbols denote the different object IDs: QSOs (filled circles); emission line galaxies (filled squares); absorption line galaxies (open squares); non-IDs (open triangles); unobserved objects (crosses).

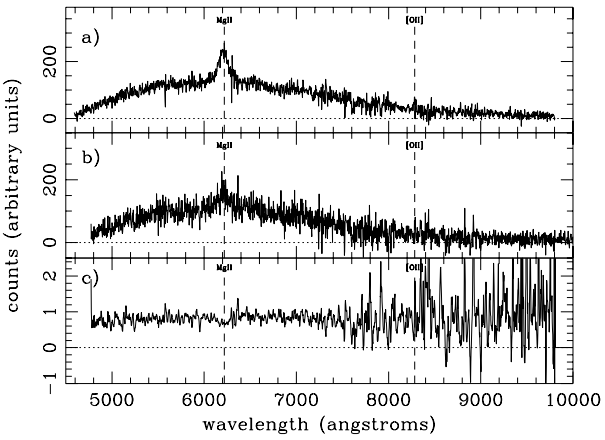

Figure 7. spectra of the QSO pair found in our KX sample KX4 (a) and KX10 (b) with emission lines denoted by the dashed lines. c) shows the flux ratio KX10/KX4 boxcar smoothed with a window of 5 pixels.

4 DISCUSSION

4.1 Blue candidates, $V - J < 3$

We can draw some preliminary conclusions on the basis of the spectroscopy completed so far. Only two sources brighter than $K = 19.5$ were found to be UVX and not KX. The UV, optical and IR colours of these two objects suggest that they are Galactic stars and spectroscopy has confirmed this in one case. The three confirmed QSOs also show a UV excess. Thus, within our sample, KX selection appears to contain all the QSOs which would have been selected via the UVX method, as we find no UVX QSOs which are not also KX. Of the 13 KX candidates with $V - J < 3$, 11 were observed, and 9 have been identified. The effective area of this sample is then 48 arcmin^2 multiplied by 9/13. (We obtain a very similar effective area if we consider the identified fraction of objects with a stricter stellarity cut > 0.8). This gives us a lower limit to the surface density of QSOs brighter than

Table 3. The two UVX non-KX sources with $K \leq 19.5$ in our survey area

name	RA(J2000)	Dec.(J2000)	U	B	V	R	J	K	S/G_K
UVX1	3 32 30.58	–27 44 59.8	19.75	20.01	19.56	19.20	18.76	18.48	0.98
UVX2	3 32 44.08	–27 48 24.4	19.50	19.93	19.37	18.92	18.51	18.15	0.98

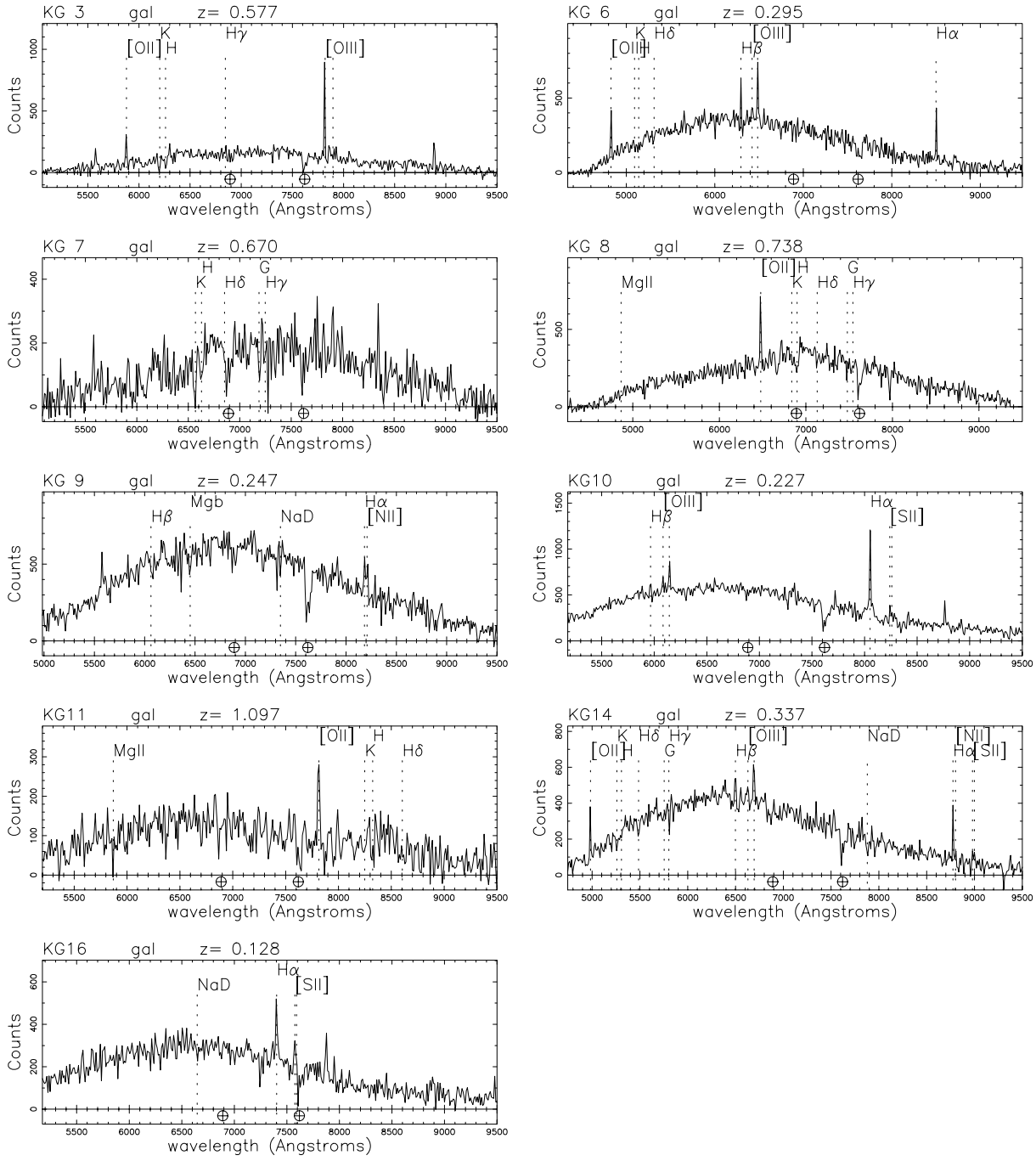

Figure 5. Spectra of the identified objects in the galaxy sample.

Table 4. $K \leq 19$ galaxies observed in addition to our KX survey. The format is the same as that in Table 1. The '?' after the [O III] for KG3 indicates that the features associated with the [O III] line are questionable due to the peculiar line ratios of the two [O III] lines. The '(abs)' after an Mg II indicates that this line is seen in absorption.

name	RA(J2000)	Dec.(J2000)	U	B	V	R	J	K	S/G_K	z	ID	spectral features
KG1	3 32 10.62	−27 47 02.0	24.58	24.77	23.43	22.21	20.19	18.42	0.07	0.000	?	
KG2	3 32 10.81	−27 46 28.0	-	-	-	24.57	20.18	18.34	0.03	0.000	?	
KG3	3 32 11.45	−27 46 50.2	24.39	24.28	22.57	21.86	19.86	18.54	0.43	0.577	gal(e)	[O II],H,K,Hγ,[O III] ?
KG4	3 32 11.55	−27 47 13.2	22.84	23.33	22.39	21.56	19.64	17.74	0.03	0.000	?	
KG5	3 32 14.87	−27 47 38.5	25.16	25.46	23.79	22.80	20.43	18.90	0.45	0.000	?	
KG6	3 32 21.79	−27 44 42.4	21.82	22.41	21.40	20.96	19.90	18.97	0.01	0.295	gal(e)	[O II],H,K,Hδ,Hβ,[O III],Hα
KG7	3 32 22.02	−27 46 56.2	22.78	23.91	22.64	21.49	19.02	17.37	0.04	0.670	gal(a)	H,K,Hδ,G,Hγ
KG8	3 32 22.63	−27 44 26.0	22.06	22.55	21.82	20.94	19.02	17.39	0.03	0.738	gal(e)	Mg II(abs),[O II],H,K,Hδ,G,Hγ
KG9	3 32 28.04	−27 46 39.5	22.26	22.18	20.68	19.86	17.94	16.23	0.08	0.247	gal(a)	Hβ,Mgb,NaD,Hα,[N II]
KG10	3 32 34.16	−27 47 12.4	21.85	22.28	21.30	20.80	19.74	18.38	0.10	0.227	gal(e)	Hβ,[O III],Hα,[S II]
KG11	3 32 39.92	−27 47 15.3	22.43	23.34	22.74	22.21	20.54	18.91	0.01	1.097	gal(e)	Mg II(abs),[O II],H,K,Hδ
KG12	3 32 42.59	−27 43 47.4	22.76	23.58	22.25	21.68	21.51	18.82	0.00	0.000	?	
KG13	3 32 42.85	−27 46 05.9	22.05	22.60	21.89	20.88	19.36	17.65	0.04	0.000	?	
KG14	3 32 45.66	−27 45 54.9	21.65	22.30	21.18	20.50	19.53	18.00	0.01	0.337	gal(e)	[O II],H,K,Hδ,G,Hγ,Hβ,[O III],
KG15	3 32 45.69	−27 44 05.9	22.20	22.93	22.15	21.12	19.91	18.33	0.02	0.000	?	NaD,Hα,[N II],[S II]
KG16	3 32 46.60	−27 47 08.9	22.15	22.51	21.46	20.85	19.98	18.90	0.00	0.128	gal(e)	NaD,Hα,[S II]

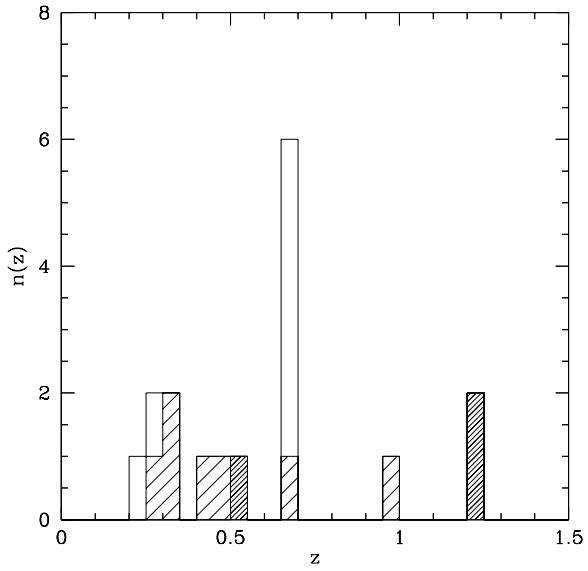

Figure 8. The redshift distribution of our KX sample. Heavy shading denotes the QSOs, light shading the narrow emission line galaxies and no shading for the absorption line galaxies. Note that most of the early type galaxies are at $z \simeq 0.66$.

$K = 19.5$ of 325^{+316}_{-177} deg^{-2}, the lower limit allowing for the possibility that the red sample contains one or more QSOs.

We can calculate the number of QSOs expected in this field, based on previous results from blue selected surveys. Taking the result of Boyle, Jones & Shanks (1991), who find a density of 76.8 QSOs per square degree at $z < 2.9$ and $B < 22$, an average $(B-K)$=3.0 and a faint end number counts slope (extrapolated) of 0.3, we expect to find ~ 1.4 QSOs in our 48 arcmin^2 field. Given the small numbers and the uncertainties in this calculation we conclude that our data are consistent with this.

Five of the KX candidates are narrow emission line galaxies. These could be obscured AGN, where the broad line region is enshrouded in dust. However, a more likely explanation, is that they are simply star forming galaxies. The current spectra are not of sufficient quality to differentiate between these two possibilities. However, galaxy evolution models (e.g. see Eisenhardt et al. 2000) suggest that late type galaxies should lie in this region of colour-colour space. Comparison with the deep *Chandra* X-ray imaging data soon to be available in this field can answer this question.

The QSO pair at $z = 1.22$ is unexpected given the small size of the sample, and the large angular separation ($> 2'$) is significantly larger than any confirmed gravitationally lensed pair. The discovery of a galaxy cluster at $z = 0.66$ may provide a foreground lens for this source, however a lens of $\sim 2'$ separation would typically require a cluster with a velocity dispersion ~ 1500kms^{-1} (assuming a simple singular isothermal sphere potential) which is exceptionally large. Again, the question of this unlikely event will be resolved with the availability of the deep *Chandra* data, which will easily detect hot gas from the cluster if it is sufficiently massive to strongly lens a background QSO.

4.2 Red candidates, $V - J \geq 3$

Of the 41 KX candidates with $V - J \geq 3$, 22 were observed, and 8 have been identified, all as galaxies. The effective area of the search for red QSOs is therefore 9.4 arcmin^2. (This could be considered an underestimate, since QSOs are easier to identify than early-type galaxies – which appear to dominate the red sample – so the 14 objects with unidentified spectra are most likely to be galaxies.) Our spectroscopy of red candidates therefore gives only a weak upper limit on the number of red QSOs of 1150 deg^{-2} (2σ).

To conclude, our preliminary spectroscopic results confirm that UVX selection is contained by KX selection, and our small sample provides a measurement of the surface density of QSOs brighter than $K = 19.5$. However our results do not yet provide useful statistics on the number of red QSOs. We plan to obtain near-infrared spectroscopy, combined with further optical spectroscopy, and an analysis of the *Chandra* image, in pursuit of this goal. As anticipated (and as also encountered with UVX surveys) contamination by galaxies is a problem for faint optical/near-infrared surveys for QSOs. With forthcoming wide-field near-IR surveys to moderate depths $K_{\rm lim} \simeq 17$, where contamination from galaxies is much less pronounced, the KX method is an obvious choice to construct unbiased samples of QSOs.

acknowledgements

This paper was prepared using the facilities of the STARLINK node at the Imperial College of Science, Technology and Medicine. We thank the ESO Imaging Survey team for making their data publicly available. SMC acknowledges the support of PPARC.

REFERENCES

Antonucci R., 1993, ARAA, 31, 473
Almaini O., Boyle B. J., Griffiths R. E., Shanks T., Stewart G. C., Georgantopoulos I., 1995, MNRAS, 277, L31
Binney J., Merrifield M., 1998, 'Galactic Astronomy', Princeton University Press
Bertin E., Arnouts S., 1996 AASup, 117, 393
Boissé P., Le Brun V., Bergeron J., Deharveng J-M., 1998, AA, 333, 841
Boyle B. J., Almaini O., Georgantopoulos I., Blair A. J., Stewart G. C., Griffiths R. E., Shanks T., Gunn K. F, 1998, MNRAS, 297, L53
Boyle B. J., Fong R., Shanks T., Peterson B. A., 1990, MNRAS, 243, 1
Boyle B. J., Jones L. R., Shanks T., 1991, MNRAS, 251, 482
Croom S. M., Smith R. J., Boyle B. J., Shanks T., Loaring N. S., Miller L., 2001, MNRAS, 322, L29
Eisenhardt P., et al., 2000, astro-ph/0002468
Fall S. M., Pei Y. C., 1993, ApJ 402, 479
Glazebrook K., Bland-Hawthorn J., 2001, PASP, 113, 197
Madau P., Ghisellini G., Fabian A. C., 1994, MNRAS, 270, L17
Rengelink R., Nonino M., da Costa L., Zaggia S., Erben T., Benoist C., Wicenec A., Scodeggio M., Olsen L. F., Guarnieri D., Deul E., Hook R., Moorwood A., Slijkhuis R., 1998, astro-ph/9812190
Schmidt M., Green R. F., 1983, ApJ, 269, 352
Warren S. J., Hewett P. C., Foltz C. B., 2000, MNRAS, 312, 827
Webster R. L., Francis P. J., Peterson B. A., Drinkwater M. J., Masci F. J., 1995, Nature, 375, 469